Journal of Materials Chemistry A

ROYAL SOCIETY OF CHEMISTRY

PAPER

View Article Online
View Journal

Cite this: DOI: 10.1039/d5ta07361h

Hydrogen-bonding ability induces structural flexibility in a zeolitic-imidazolate framework (ZIF-71)

J. Farrando-Pérez,[a] A. Missyul,[b] J. J. Gutiérrez-Sevillano,[c] S. Calero,[cd] C. Carrillo-Carrión,[e] A. Martin-Calvo[c] and J. Silvestre-Albero*[a]

Received 9th September 2025
Accepted 7th December 2025

DOI: 10.1039/d5ta07361h

rsc.li/materials-a

The structural flexibility of ZIF-71 has been evaluated using a series of probe molecules with different chemical characteristics. Liquid-phase adsorption processes in aqueous media confirm that the studied analytes (aniline, phenol, benzoic acid, benzaldehyde, 4-fluoroaniline, toluene, fluorobenzene and chlorobenzene) can be classified into two groups, *i.e.*, those with high accessibility (uptake above 200 mg g^{-1}) and those with limited accessibility (approximately 10–20 mg g^{-1}, *i.e.*, one order of magnitude lower). Synchrotron X-ray powder diffraction measurements reveal that the limited uptake for certain probes is attributed to a phase transition, from the open-pore (op), ZIF-71 phase, to the narrow-pore (np), ZIF-72 phase. Interestingly, this irreversible phase transition is exclusively promoted by probes containing highly polar functional groups. Monte Carlo simulations suggest that the observed behavior cannot be fully justified by intermolecular interactions and/or water–probe interactions, but is instead driven by the hydrogen-bonding ability of the analytes. In other words, the phase transition occurs exclusively in the presence of analytes possessing strong hydrogen-bonding ability. These hydrogen-bonding interactions appear to facilitate water penetration into the otherwise hydrophobic inner cavities of ZIF-71, thereby accelerating the kinetically controlled transition from ZIF-71 (open-pore) to ZIF-72 (narrow-pore).

Introduction

Although porous materials such as activated carbons, zeolites, and metal–organic frameworks, among others, are traditionally considered rigid solids, *operando* techniques and theoretical predictions have suggested that some are able to experience structural flexibility under an external stimulus (variations in pressure, temperature, *etc.*).[1–3] The extent of these changes depends on the structural characteristics of the host material (*e.g.*, skeleton density, intracrystalline interactions, *etc.*) and the magnitude of the stress applied. One of the most widely investigated phenomena is the structural change induced by adsorption, commonly referred to as adsorption-induced deformation. Investigation of the interplay between adsorption and structural deformation under *operando* conditions is of paramount importance to understand the performance of porous materials under different scenarios, with the associated challenges and opportunities (*e.g.*, for selective separation processes).

The reported structural dynamics for activated carbon materials, clays, coal and zeolites (*e.g.*, Ge-containing zeolites) are generally limited (adsorption-induced strain <0.5%), yet they can significantly impact molecular diffusion dynamics.[4,5] Consequently, these can be considered as "relatively rigid" frameworks. These small dimensional changes can be rationalized by the adsorption stress model introduced by Ravikovitch and Neimark, *i.e.*, molecules adsorbed on the inner cavities of porous materials exert a large internal stress (on the order of megapascals), which is reflected in an elastic deformation of the matrix.[6,7] Interestingly, these adsorption-induced deformations are significantly larger for metal–organic framework materials (MOFs) and, more specifically, for a subfamily known as zeolitic-imidazolate frameworks (ZIFs).[1] Although structurally similar to zeolites (*e.g.*, the M–Im–M angle is similar to the Si–O–Si angle), ZIFs are endowed with greater framework flexibility upon adsorption, in addition to other advantageous properties such as hydrothermal stability and high adsorption capacity. These structural dynamics are traditionally associated with pore breathing phenomena, gate-opening effects, and both reversible and irreversible phase transitions, depending on the

[a]*Advanced Materials Laboratory, Department of Inorganic Chemistry-, Materials University Institute of Alicante, University of Alicante, Spain. E-mail: joaquin.silvestre@ua.es*

[b]*CELLS-, ALBA Synchrotron, Cerdanyola del Vallés, Barcelona, Spain*

[c]*Center for Nanoscience and Sustainable Technologies (CNATS), Dpt Physical, Chemical and Natural Systems, Universidad Pablo de Olavide, Seville, Spain*

[d]*Department of Applied Physics, Eindhoven University of Technology, Eindhoven, The Netherlands*

[e]*Institute for Chemical Research (IIQ), CSIC-, University of Seville, Spain*

framework topology, pore size/shape and the guest molecule used.[8–18] For instance, ZIF-7 can exist in two different phases: large pore (lp) and narrow pore (np), and can even adopt an extra-large pore (xlp), depending on the sample environment.[11,12] While these structural changes are well-identified for gas-phase adsorption processes, their extrapolation to liquid-phase adsorption processes is not straightforward. In liquid solutions, the adsorption performance and the associated potential structural changes are more complex, as they depend not only on host–guest interactions, but also on solvent properties such as polarity, solubility and temperature, including solvent–host and solvent–guest interactions. Understanding these competitive processes is essential for predicting the performance of these ZIFs in liquid-phase applications, including their role as heterogeneous catalysts.[19] The majority of studies reported in the literature have been restricted to the evaluation of the structural changes with pure components (*e.g.*, water) upon intrusion at high pressures (*i.e.*, tens of MPa).[20,21] For instance, Sun and coworkers evaluated the structural flexibility of ZIF-8 upon intrusion/extrusion cycles.[21] These studies demonstrated that structural flexibility is preserved when using non-wetting penetrating liquids, although high pressures are needed to deform the ZIF framework. Unfortunately, the structural response of ZIFs under competitive adsorption conditions (*i.e.*, simultaneous presence of guest and solvent) has been scarcely evaluated in the literature.

Recent studies using a double chlorinated ZIF such as ZIF-71 have suggested that structural dynamics are highly influenced by the nature of the probe molecule evaluated in aqueous solutions.[22] While a chlorinated molecule such as chlorobenzene is adsorbed with a high uptake, a similar probe such as phenol is completely excluded from the ZIF-71 framework (one order of magnitude lower uptake with water as a solvent). Although this performance could *a priori* be related to specific Cl–Cl interactions at the interface, synchrotron X-ray diffraction measurements in the pristine and used samples confirmed that the adsorption performance was defined by an irreversible phase transition from an open-pore (op) structure, ZIF-71, to a narrow-pore (np) structure, ZIF-72. Despite these findings described so far, the real mechanism defining the adsorption performance of ZIF-71 *vs.* different volatile organic compounds (VOCs) and the associated structural changes is still unclear. With these premises in mind, in this manuscript we want to extend these studies to new probes with different characteristics (polarity, solubility, boiling point, *etc.*), to correlate structural transformations in ZIF-71 with the physicochemical properties of the aqueous environment.

Experimental section

MOF synthesis

ZIF-71 was synthesized following the procedure previously described in the literature.[22] Briefly, the synthesis was performed using zinc acetate ($Zn(CH_3COO)_2 \cdot 2H_2O$, Sigma-Aldrich 99.99%) as a metallic precursor and 4,5-dichloroimidazole (Thermo Scientific Chemicals, 98%) as a linker, with methanol as a solvent. ZIF-71 was synthesized under stirring conditions and at atmospheric pressure by mixing both solutions (metal and linker dissolved in 150 mL methanol) for 24 h. After decanting the suspension to remove the methanolic supernatant, the recovered ZIF-71 crystals were left to soak in chloroform (25 mL, two successive portions) for 48 h. The purified solid was then separated by filtration and, finally, dried under vacuum at 100 °C for 24 h.

Textural characterization

The textural properties of the synthesized ZIF were evaluated using nitrogen adsorption at cryogenic temperatures (−195 °C). Adsorption measurements were performed in home-built manometric equipment designed and constructed by our research group. Prior to adsorption experiments, ZIF-71 was degassed under ultra-high vacuum (UHV) at 150 °C for 12 h.

Synchrotron X-ray powder diffraction (SXRPD) measurements

SXRPD measurements of the synthesized ZIF-71 and the different samples subjected to adsorption tests were performed at the ALBA synchrotron – MSPD station (Spain). These experiments were performed on the powder samples using a thin silica capillary (i.d. 0.7 mm), using a MYTHEN detector and a wavelength of 0.6204 Å (20 keV). For the used samples (upon completion of the liquid-phase adsorption test), these were filtered and dried at RT for 2 days before the SXRPD measurements.

Liquid-phase adsorption experiments

The adsorption performance of ZIF-71 towards selected volatile organic compounds (VOCs) was quantified using UV-vis spectroscopy, using a previously constructed calibration curve for each analyte. Liquid-phase adsorption experiments were limited by the low solubility of some of the selected probes in aqueous media. Aqueous solutions with an initial concentration of 50 ppm (50 mL total volume) were used for all the probes, except for toluene, chlorobenzene and fluorobenzene, where initial concentrations up to 250 ppm were tested due to their adsorption performance. Briefly, each experiment was performed with 50 mg of ZIF-71, using closed glass vials containing 50 mL of each analyte solution. Vials were stirred at room temperature until equilibrium was reached. Before each experiment, ZIF-71 samples were *ex situ* outgassed at 150 °C, overnight (*i.e.*, thermal activation). Aliquots were taken at different time intervals and analyzed by UV-vis spectroscopy, recording the absorbance value at the wavelength corresponding to the maximum absorbance of each analyte ($\lambda_{max} = 211$ nm (chlorobenzene), 270 nm (phenol), 260 nm (toluene), 258 nm (fluorobenzene), 246 nm (benzaldehyde), 281 nm (aniline), 273 nm (benzoic acid) and 287 nm (4-fluoroaniline)).

Simulation details

Monte Carlo simulations were carried out to evaluate, at the molecular level, the interactions between probe molecules and the ZIF-71 framework in aqueous solutions. Simulations were performed using the RASPA 2.0 code.[23] We used the canonical

ensemble (NVT) accounting for the number of molecules of each probe to be in the liquid state within an empty box with a side length of 30 Å, as a single component and at 50 ppm in aqueous solution. To ensure that the systems reach equilibrium, 800k cycles (following 80k initialization cycles) were used together with random moves applied to randomly selected molecules (rotation, translation, insertion and deletion, and identity change in the case of aqueous solutions). A max(N, 20) of attempted moves were performed on each cycle, where N is the number of molecules. To evaluate the strength of the interaction between the probe molecules and ZIF-71, enthalpies of adsorption at low coverage were calculated using the Widom test-particle insertion method.[24] For improved statistical reliability, each calculation was performed 6 times per probe molecule, and the results were then averaged. Details of the ZIF-71 structure as well as Lennard-Jones parameters and partial charges can be found in our previous work.[22] All guest molecules and water were modeled as rigid entities using rigid full atom models with atomic positions and point charges taken from PubChem,[25] and Lennard-Jones parameters from TraPPE.[26] The extended simple point charge (SPC/E) model was used for water.[27] Atomic interactions within the system were described through Lennard-Jones (L-J) and coulombic potentials that are cut and shifted at a cut-off distance of 12 Å. Lorentz–Berthelot mixing rules were used for cross-term L-J interactions, while the Ewald summation method (with a relative precision of 10^{-6}) was used for the electrostatic interactions. To avoid finite-size effects, we use periodic boundary conditions and a simulation box with a, b, and c lengths at least twice the cut-off. Since we applied a cut-off distance of 12 Å for the potentials (beyond that distance the potentials are truncated and shifted) and the unit cell of the empty box (30 × 30 × 30 Å) and ZIF-71 are larger than 28 × 28 × 28 Å, the simulation box consists of just one unit cell. This simulation protocol provides a consistent and computationally efficient method to rank the accessibility of different probe molecules into ZIF-71 and to identify the dominant factors (*e.g.*, size, polarity, and H-bonding potential) controlling guest–host interactions.

Results and discussion

The physicochemical properties of the synthesized ZIF-71 have been characterized previously.[22] Briefly, ZIF-71 is a dichlorinated zeolitic imidazolate framework composed of Zn^{2+} centers linked by 4,5-dichloroimidazolate ligands (see Fig. 1). ZIF-71 is a purely microporous material, exhibiting an apparent BET surface area of around 1060 $m^2\ g^{-1}$, in accordance with the predicted cubic topology featuring large α-cages (*ca.* 1.6 nm) connected through eight-, six- and four-membered ring windows. Pore size distribution obtained after application of the NLDFT model reveals two main maxima at *ca.* 1.4 and 1.6 nm, assigned to the distinct microporous cages present in the ZIF-71 structure. These structural features closely match theoretical GCMC simulations, confirming the effectiveness of the synthesis procedure applied. Previous studies described in the literature have identified an anomalous adsorption behavior of ZIF-71 in aqueous-phase environments. For

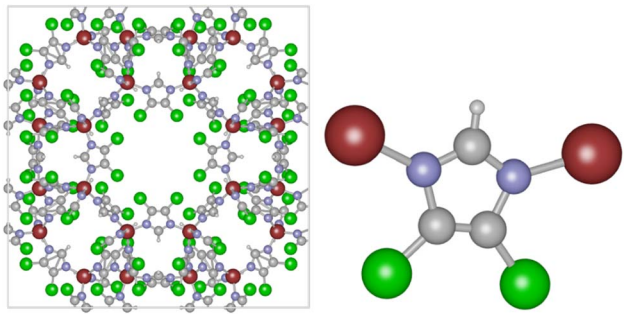

Fig. 1 Atomic structure of ZIF-71. Zinc atoms are shown in red, carbon atoms in gray, nitrogen atoms in blue, chlorine atoms in green, and hydrogen atoms in white.

instance, as described above, the adsorption performance for two structurally similar volatile organic compounds (phenol and chlorobenzene), but with different polarity, highly differed. While chlorobenzene was characterized by fast adsorption kinetics (<90 min) and a high adsorption uptake (above 200 mg g^{-1}), phenol adsorption was kinetically slow (>25 h) and exhibited a limited adsorption capacity at equilibrium (less than 10 mg g^{-1}). To shed further light on this unexpected behavior, these liquid-phase adsorption tests have been extended to a broader range of benzene derivatives bearing diverse functional groups (–OH, –COOH, –F, –Cl, –COH, $–CH_3$ and $–NH_2$), all sharing the same backbone, the aromatic benzene ring. The introduction of these substituents modifies the physicochemical properties of the benzene derivatives, in terms of: (i) conformational flexibility, (ii) steric/electronic parameters, (iii) solubility, and (iv) polarity, among others, which may in turn influence their adsorption performance. Table 1 summarizes the key properties and molecular formulas of the selected probes.

The selected probes share a common benzene backbone, while the nature of the functional group imparts distinct physicochemical properties such as bond enthalpy, electronegativity and polarizability. The selected probes span from halogenated organics, with highly electronegative functional groups and strong C–X bonds, to nitrogen- and oxygen-functionalized benzene derivatives, characterized by their high boiling points due to the presence of strong intermolecular interactions. Once the target molecules were selected, their adsorption kinetics on ZIF-71 as the guest material were tested at 25 °C. All adsorption experiments were performed using 50 mL of aqueous solutions at a concentration of 50 ppm, except for toluene, chlorobenzene and fluorobenzene, for which a concentration of 250 ppm was used instead due to their high adsorption capacity.

As shown in Fig. 2, ZIF-71 exhibits good adsorption performance for toluene, chlorobenzene and fluorobenzene. In all cases, the amount adsorbed approaches 230–250 mg g^{-1} and is associated with extraordinary fast kinetics for all these three molecules. These results suggest that, independently of the characteristics of the functional group incorporated (*e.g.*, different electronegativity of the functional group) and,

Table 1 Physicochemical properties of the probe molecules evaluated, including molecular formula, connecting bond type and enthalpy, electronegativity of the bonding atom, and boiling point. These parameters are discussed in relation to their influence on the adsorption behavior in ZIF-71

Probe	Formula	Connecting bond[a]	Bond energy[b] (kJ mol^{-1})	Electronegativity[c]	Boiling point (°C)
Fluorobenzene	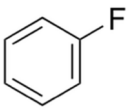	C–F	485	3.98	85
Chlorobenzene	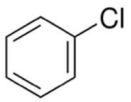	C–Cl	328	3.16	132
Toluene	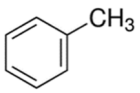	C–C	348	2.55	110.6
Aniline	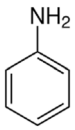	C–N	293	3.04	184.1
Phenol	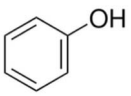	C–O	358	3.44	181.7
Benzoic acid	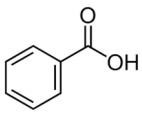	C–C	358	2.55	250
Benzaldehyde	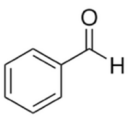	C–C	358	2.55	178.1
Fluoroaniline	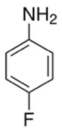	C–F C–N	485 293	3.98 3.04	188

[a] Nature of the bond connecting the benzene backbone with the incorporated functional group. [b] Enthalpy (kJ mol^{-1}) of the bond connecting the benzene backbone with the incorporated functional group. [c] Electronegativity of the atom connected to the benzene backbone.

indirectly, the polarizability of the selected molecule, the adsorption performance is rather similar. Previous theoretical studies using Grand Canonical Monte Carlo simulations have suggested that the large uptake for chlorobenzene does not relate to the presence of preferential $Cl_{molecule}$–Cl_{ZIF} interactions (host–guest interactions), but rather to the promising adsorption performance of ZIF-71 for these molecules.[22] These results are particularly relevant given the need to develop sorbents with high affinity for halogenated organic compounds (*e.g.*, chlorofluorocarbons (CFCs) or derivatives from the refrigeration sector).[28] Despite these excellent results achieved so far, Fig. 3 clearly shows that this behavior cannot be extended to other functionalized benzene derivatives such as benzaldehyde, benzoic acid, phenol, and aniline. According to the results described in Fig. 3, ZIF-71 does not significantly adsorb any of these molecules (uptake is one order of magnitude lower, *ca.* 10–20 mg g^{-1}). Despite the lower adsorption capacities, the adsorption kinetics are also fast (equilibrium is reached in less than 2 h), except in the case of phenol, when more than 25 h are needed. As described above, adsorption tests for these probes indicate that, regardless of the specific characteristics of the functional groups (*e.g.*, differences in electronegativity) and, indirectly, the polarizability of the selected molecules, the overall adsorption performance in terms of uptake remains rather similar.

The results clearly reveal two distinct groups of molecules with respect to ZIF-71 adsorption performance, *i.e.*, those probes easily adsorbed (uptake $\sim$ 250 mg g^{-1}) and those probes

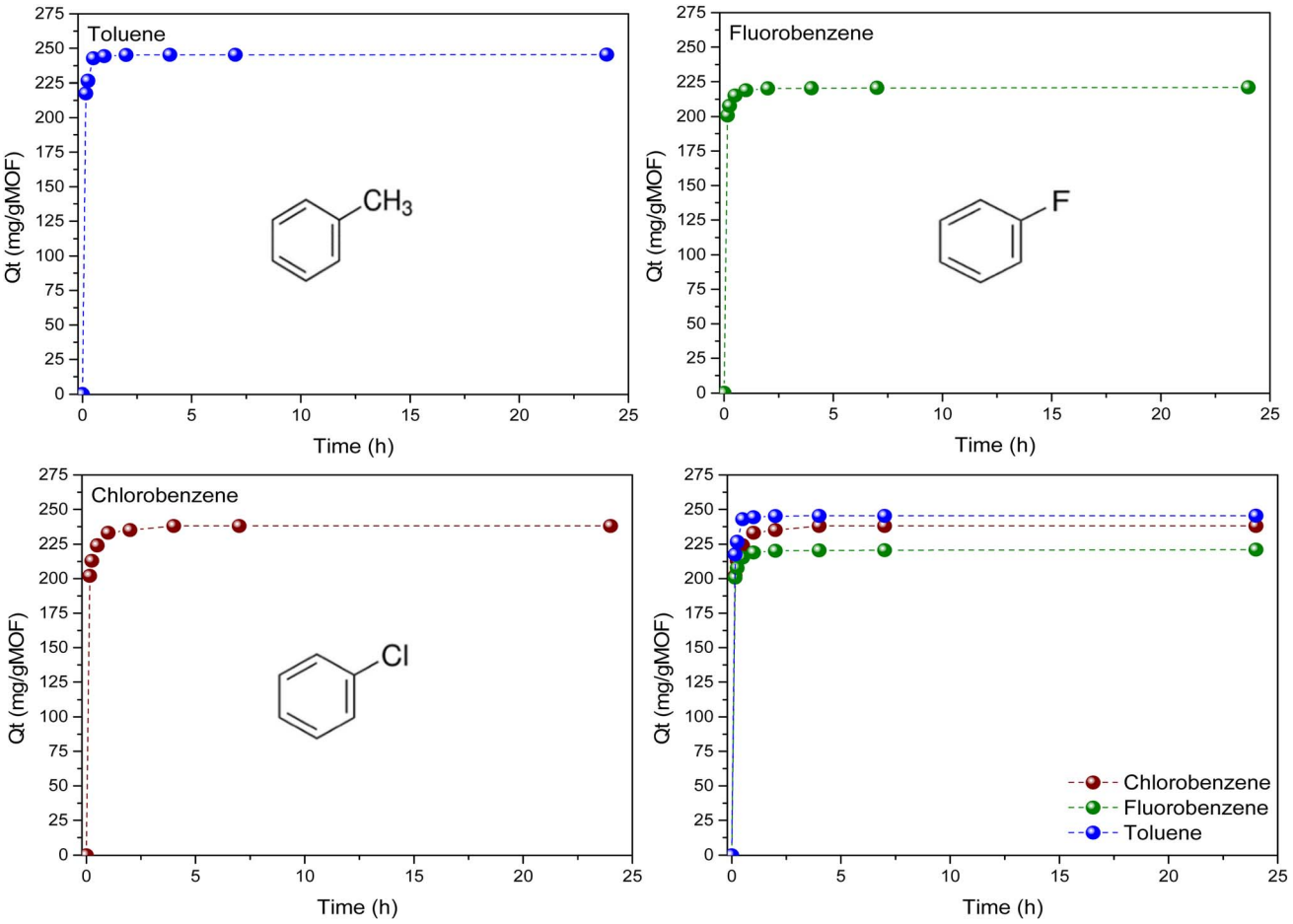

Fig. 2 Adsorption kinetics (mg g_{MOF}^{-1} *vs.* adsorption time) for toluene, fluorobenzene, and chlorobenzene at 25 °C. These experiments were performed using 50 mL of aqueous solution at a concentration of 250 ppm. A summary with all the kinetics is also included.

that are effectively "rejected" by the porous framework (uptake $\sim$ 20 mg g^{-1}). A closer look at the physicochemical properties of the tested molecules (Table 1) reveals that the observed trends cannot be readily rationalized. Neither the electronegativity of the functional group (X) nor the intrinsic characteristics of the C–X bond (strength and polarizability) appear to have a real effect on the adsorption performance of ZIF-71. In contrast, the parameters described in Table 1 nicely reflect that the non-adsorbing molecules in ZIF-71 are those with high boiling points, *i.e.*, low volatility. These observations suggest *a priori* that intermolecular interactions in the liquid phase may play a crucial role.

To gain more knowledge about this complex adsorption behavior, the study was extended to a molecule containing two different functionalities, C–F and C–NH_2, namely fluoroaniline. The open question at this stage is how ZIF-71 will perform when exposed to a molecule that combines both a functionality/property typically associated with strong adsorption (–F) and another less favorable one (–NH_2). As shown in Fig. 3, in this case, the adsorption outcome is governed by the intrinsically "non-favorable" group. Indeed, for 4-fluoroaniline, the total uptake is limited to 10 mg g^{-1}, which is even lower than that of aniline. This result indicates that the preferential molecular orientation upon adsorption is not the determining factor; rather, the intrinsic properties of the molecule itself in the aqueous media dictate the behavior. Notably, 4-fluoroaniline also exhibits a high boiling point (188 °C). Consequently, this finding further supports the hypothesis that molecular properties, such as boiling point, directly related to the presence of strong intermolecular interactions, may play a dominant role in determining the adsorption behavior, overriding the intrinsic characteristics of the functional group itself.

To further identify the mechanism behind this adsorption performance, used samples were evaluated using synchrotron X-ray powder diffraction (SXRPD) to identify potential structural changes upon adsorption. Fig. 4 shows the SXRPD patterns for the two groups of molecules evaluated (adsorbing and non-adsorbing probes). In the specific case of samples tested with toluene, chlorobenzene and fluorobenzene, SXRPD shows the typical diffraction pattern of pure ZIF-71, with main peaks at 2θ values of 1.73°, 2.47°, 3.04°, 3.49°, 6.33°, 6.79° and 7.47°.

The scenario changes significantly upon adsorption of the other probes. As shown in Fig. 5, synchrotron XRD patterns suggest the appearance of new peaks, attributed to a new phase, ZIF-72 (with the main peaks at 2θ values of 4.43°, 5.11°, 6.77°, 7.24°, 8.49°, 10.24° and 11.17°). As described in the literature,

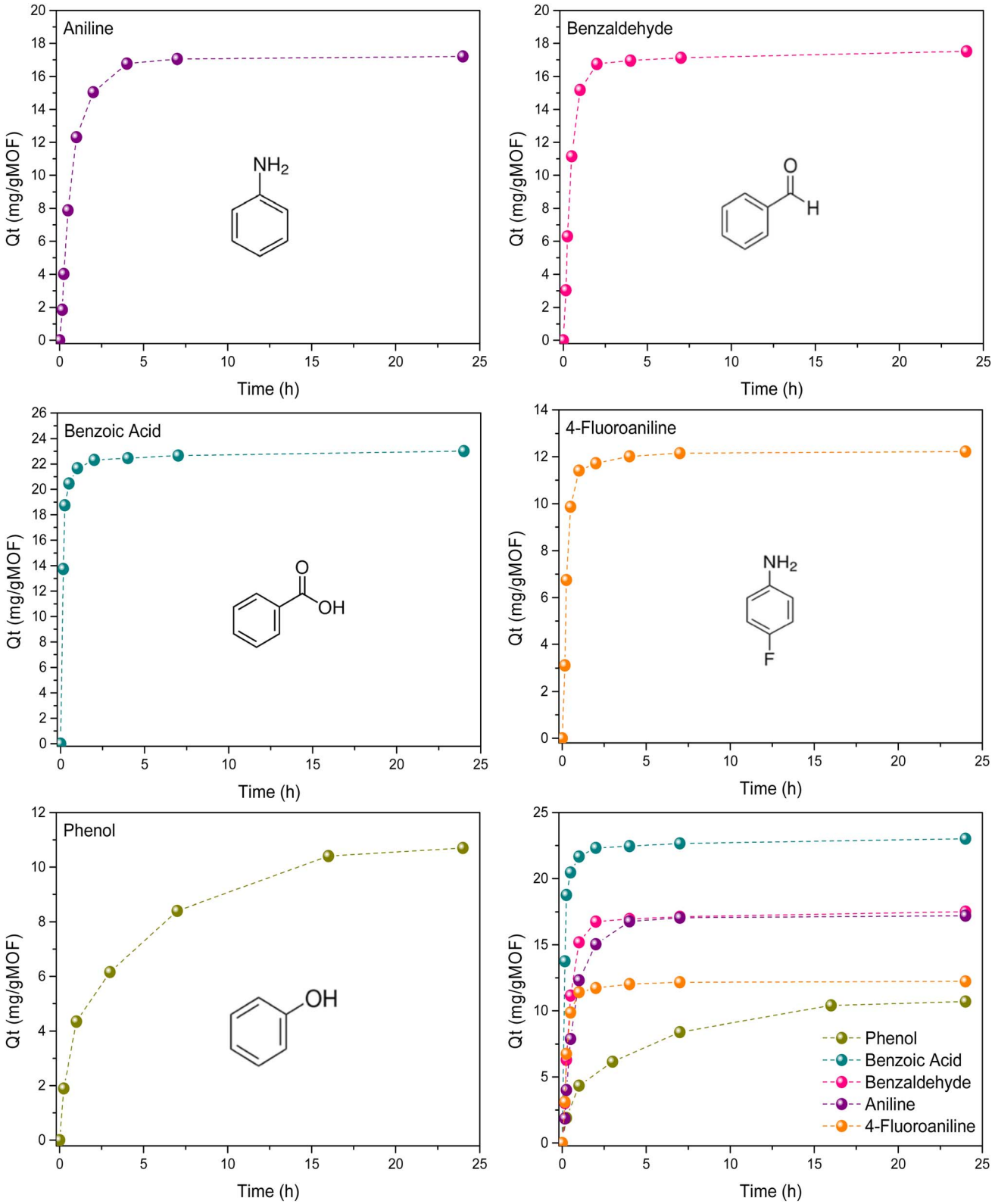

Fig. 3 Adsorption kinetics (mg g_{MOF}^{-1} *vs.* adsorption time) for aniline, benzaldehyde, benzoic acid, 4-fluoroaniline and phenol at 25 °C. These experiments were performed using 50 mL of aqueous solution at a concentration of 50 ppm. A summary with all the kinetics is also included.

ZIF-72 corresponds to a highly dense ZIF phase with a small surface area (*ca.* 35 m^2 g^{-1}, based on GCMC simulations) and with a pore aperture of approximately 0.2 nm, significantly smaller than the kinetic diameter of the selected probes (even smaller than the kinetic diameter of water molecules). This observation likely accounts for the low adsorption uptake

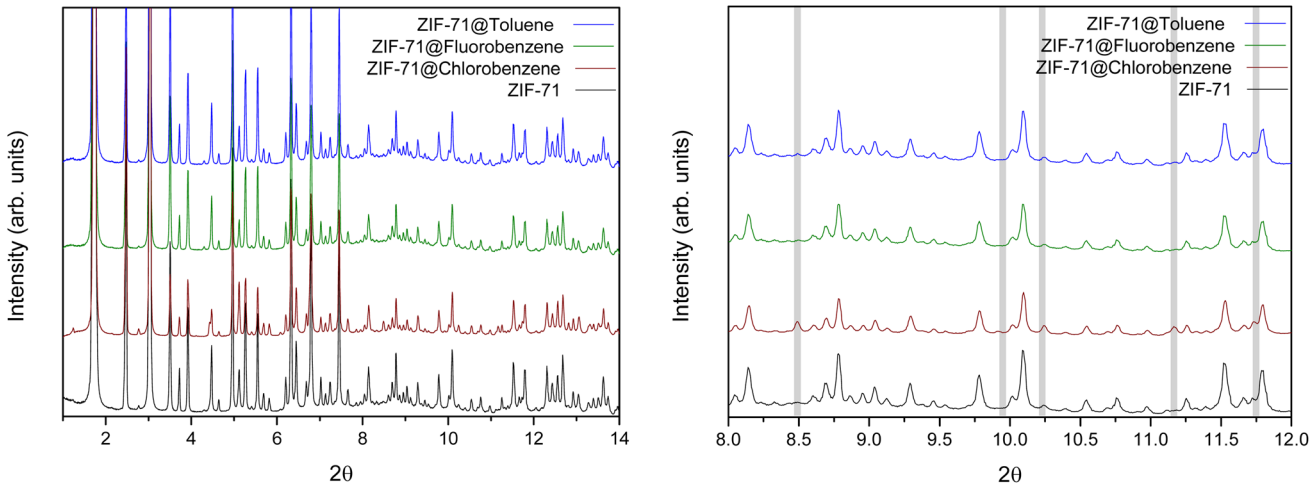

Fig. 4 (Left) Synchrotron XRPD pattern of pristine ZIF-71 and the same material after adsorption of toluene, fluorobenzene and chlorobenzene at 25 °C; (right) inset showing a detailed analysis of the 2θ range: 8.0–12.0°, with bars (grey color) to identify the theoretical position for peaks associated with the narrow-pore ZIF-72.

identified for these probes. A closer examination of Fig. 5 shows that the ZIF-71 to ZIF-72 phase transition is only partial for aniline, benzaldehyde and fluoroaniline, while in the case of phenol, a significant proportion of the material converts to ZIF-72. Notably, for the specific case of benzoic acid, the phase transformation appears to be nearly complete (close to 100%), as no peaks attributed to ZIF-71 are detected. It is worth emphasizing that these probes promoting the phase transition are characterized by a high boiling point and a high polarity. Although kinetically driven, the ZIF-71 to ZIF-72 phase transition follows a discernible trend linked to the intrinsic properties of the probe, particularly the strength of intermolecular interactions in the liquid phase, likely driven primarily by hydrogen bonding.

Based on the results described so far, the nature of the evaluated probes appears to play a significant role in promoting the phase transition from ZIF-71 to ZIF-72. All these experimental observations point to the boiling point of the probe, and indirectly to the strength of the intermolecular interactions, as key parameters governing the adsorption process (for instance, benzoic acid, which exhibits the highest boiling point, promotes the phase transition to the largest extent).

To provide more light, the interaction strength of the different molecules with the ZIF-71 material has been investigated at low coverage. From the analysis of the enthalpies of adsorption, the low value obtained for water in ZIF-71 corroborates the hydrophobic nature of this material (-13.9 kJ mol^{-1}). On the other hand, the values obtained for the probe molecules evaluated indicate a stronger interaction and allow us to

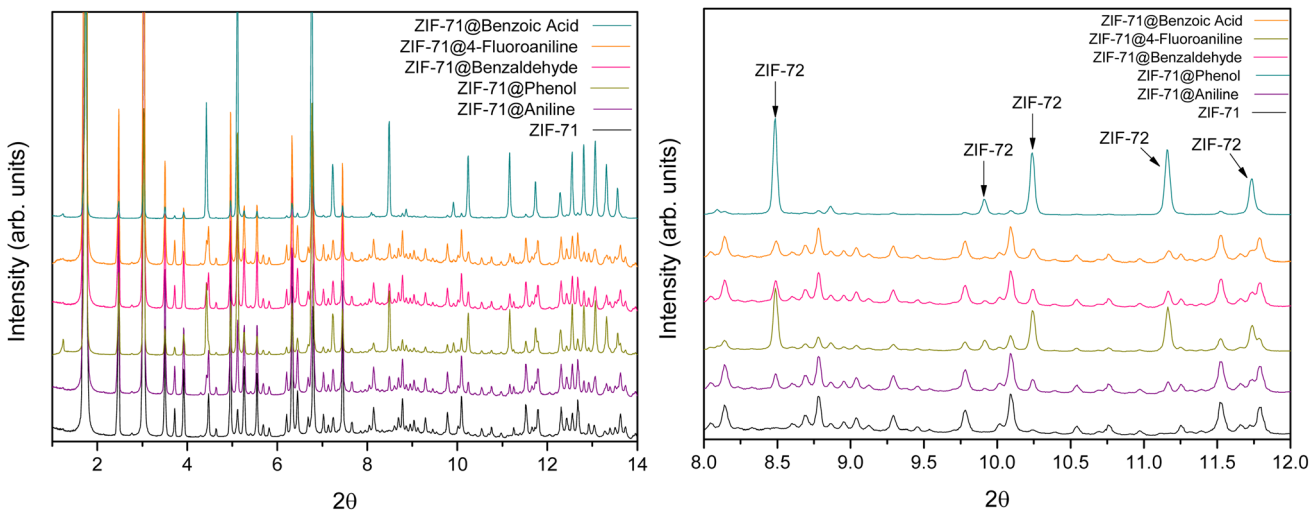

Fig. 5 (Left) Synchrotron X-ray powder diffraction of ZIF-71 before and after being used in the adsorption of benzoic acid, 4-fluoroaniline, benzaldehyde, phenol, and aniline; (right) inset showing a detailed analysis of the 2θ range: 8.0–12.0°, with arrows to identify the peaks associated with the narrow-pore ZIF-72.

differentiate the behavior inside the material. Benzoic acid exhibits the strongest interaction with ZIF-71 (−72.7 kJ mol^{-1}), followed by phenol (−66.6 kJ mol^{-1}). Toluene and aniline show comparable values (−64.8 and −63.0 kJ mol^{-1}, respectively), while chlorobenzene presents a slightly weaker interaction (−61.5 kJ mol^{-1}). The lowest interaction energies correspond to 4-fluoroaniline (−58.8 kJ mol^{-1}), fluorobenzene (−58.0 kJ mol^{-1}), and benzaldehyde (−56.4 kJ mol^{-1}). Unfortunately, these results on their own cannot be correlated with the adsorption trends observed experimentally.

Since the liquid-phase adsorption experiments are performed using H_2O as a solvent, the nature of the phase transition is more complex due to the necessity to incorporate a new component (ZIF network + solvent + probe). *A priori*, one can anticipate that the H_2O–probe and H_2O–network interactions could also play a certain role in the structural transition, although additional evidence is needed. To gain more knowledge on the H_2O–probe interactions and the potential formation of hydrogen bonding, Monte Carlo simulations in the NVT ensemble were performed for probes as single components (with N calculated to mimic the liquid density of each probe) and for 50 ppm aqueous solutions. For this purpose, the number of molecules (N) was fixed within an empty cubic box with a side length of 30 Å (V) and at room temperature (T). Table 2 reports the energetics of the intermolecular and H_2O–probe interactions under the experimental conditions applied in the liquid-phase adsorption studies (50 ppm). The water–probe interactions are summarized in Fig. 6. To facilitate the comparison of the calculated intermolecular interactions, an equal concentration of 50 ppm was considered for all the probes, regardless of their adsorption performance. A closer look at Table 2 shows that intermolecular interactions (excluding water) are high for benzoic acid, phenol, benzaldehyde and aniline, *i.e.*, all probes characterized by poor adsorption performance. In contrast, chlorobenzene, fluorobenzene and toluene are the probes with lower intermolecular interactions. These trends align well with the experimental data and the reported boiling points, although the real scenario must also consider the solvent used (water). To this end, the water–probe interaction energy was also evaluated using Monte Carlo simulations (Table 2 and Fig. 6). The strongest interactions were obtained for benzoic acid, followed by aniline, toluene, benzaldehyde and 4-fluoroaniline with similar values. In contrast, phenol, chlorobenzene and fluorobenzene showed the weakest interactions with water.

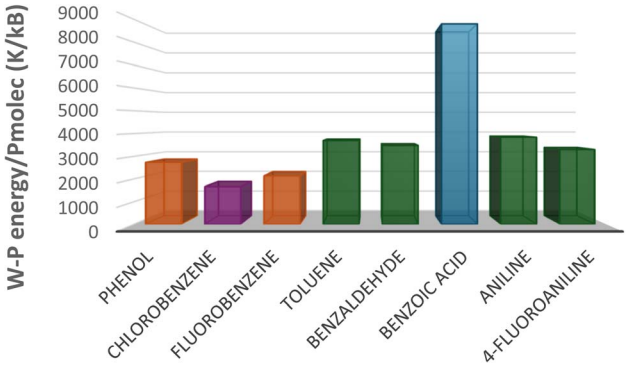

Fig. 6 Water–probe interaction energy per probe molecule (W–P/Pmolec) at 25 °C.

Unfortunately, the obtained water–probe calculations do not fully correlate with the experimental results achieved so far. While benzoic acid, aniline, benzaldehyde, and 4-fluoroaniline, with a higher interaction energy with H_2O, induce the phase transition from ZIF-71 to ZIF-72, fluorobenzene and chlorobenzene, with the lowest interaction energy, do not trigger any structural change. However, toluene with a large interaction energy and phenol with a low interaction energy with water deviate from this trend.

For a deeper understanding of the adsorption mechanism and the associated structural changes, the formation of hydrogen bonds has also been evaluated. To accurately estimate the number of hydrogen bonds between molecules, it is essential to apply a well-defined and rigorous criterion. According to the literature, various approaches have been proposed to identify hydrogen bonds based on energetic and geometric considerations.[29–33] In this study, hydrogen-bond

Table 2 Calculated interaction energies for each probe molecule, both as pure liquid components and at 50 ppm in aqueous solution. Water–probe interaction per probe molecule (W–P/Pmolec) is also reported

	Pure liquid			Aqueous solution			W–P/Pmolec
Molec	Liq density (kg m^{-3})	Particles/box	Energy (K k_B^{-1})	[Solution] (ppm)	Particles/box	Energy (K k_B^{-1})	Energy (K k_B^{-1})
Water	997	900	−5040467.5		900		
Phenol	1058	183	−1388967.9	50	9	−5133407.7	−2736.7
Chlorobenzene	1101	159	−761394.2	50	7	−5085625.4	−1662.5
Fluorobenzene	1019	172	−685626.1	50	8	−5089422.7	−2133.2
Toluene	862	152	−672182.2	50	9	−5113513.9	−3694.0
Benzaldehyde	1043	160	−1257230.9	50	8	−5131125.5	−3474.6
Benzoic acid	1075	143	−1782693.9	50	7	−5189347.0	−8802.1
Aniline	1017	178	−1055691.4	50	9	−5128379.1	−3837.1
4-Fluoroaniline	1173	172	−962191.8	50	7	−5102712.2	−3298.0

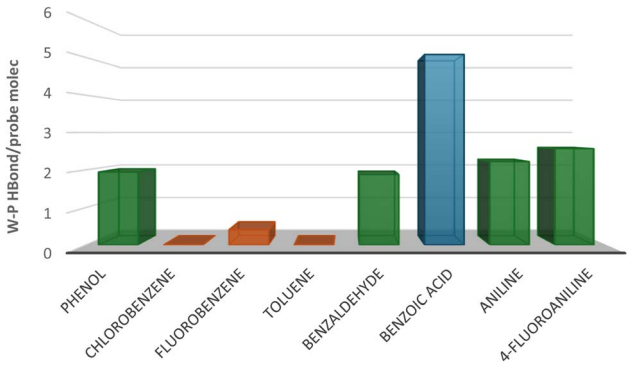

Fig. 7 Water-probe hydrogen bonds per probe molecule (W–P/Pmolec) formed on each 50 ppm aqueous solution at 25 °C.

formation was analyzed using a geometric criterion. In this approach, a hydrogen bond between two molecules is considered to exist when the interatomic distances rOO and rOH are below specific cutoff values of 3.6 Å and 2.45 Å, respectively. Furthermore, the angle α, defined between the intermolecular O–O vector and the covalent O–H bond, must fall within a predefined angular limit of 30°. Fig. 7 shows the number of hydrogen bonds formed per probe molecule in 50 ppm aqueous solutions. As can be observed, benzoic acid exhibits the highest hydrogen-bonding capacity with water (5.1 HB/Pmolec), far exceeding that of 4-fluoroaniline, aniline, phenol and benzaldehyde (2.6, 2.2, 1.9, and 1.8 HB/Pmolec, respectively). In contrast, fluorobenzene is by far the probe with the lowest hydrogen-bonding capacity with water (0.4 HB/Pmolec), while toluene and chlorobenzene do not form hydrogen bonds at all. These results perfectly fit with the adsorption data described above and clearly identify two groups of molecules: (i) phenol, benzaldehyde, benzoic acid, aniline and fluoroaniline, with hydrogen-bonding ability (W–P/Pmolec) greater than 1, and (ii) chlorobenzene, fluorobenzene and toluene, with a hydrogen bonding ability (W–P/Pmolec) below 1 or nearly zero. Furthermore, the markedly higher hydrogen-bonding ability predicted for benzoic acid is consistent with the nearly complete phase transition (~100%) observed experimentally by synchrotron XRPD.

Exploratory molecular dynamics simulations were conducted to assess possible diffusive behavior inside ZIF-71. Only chlorobenzene and benzaldehyde exhibited an incipient slope in the mean-square displacement, while the remaining molecules remained sub-diffusive over tens of nanoseconds. Given these extremely slow dynamics under aqueous conditions, no meaningful diffusion coefficients could be extracted, and the analysis is therefore restricted to adsorption thermodynamics, which dominate the overall sorption behavior.

The adsorption mechanism predicted by Monte Carlo simulations perfectly agrees with previous studies described in the literature.[22] Although ZIF-71 is a highly hydrophobic material with a poor water adsorption uptake, the formation of hydrogen bonds with some specific analytes must be the mechanism that promotes water to access the inner cavities, thus speeding up the phase transition from ZIF-71 to ZIF-72. Previous studies using inelastic neutron scattering (INS) and synchrotron X-ray powder diffraction (SXRPD) have shown that water molecules remain trapped in the inner cavities of the ZIF after the phase transition (even after evacuation under ultra-high vacuum conditions), confirming that H_2O acts as the catalyst for this irreversible phase transformation.[22,34] Once ZIF-71 is converted to ZIF-72, water molecules cannot evaporate and/or desorb from the material due to the small pore size aperture in ZIF-72 (around 0.2 nm).

Furthermore, these INS studies suggested that the phase transition must be initiated at the external surface of the ZIF-71 microcrystals and further propagate to the inner core over time.[22] This hypothesis is fully consistent with the observed adsorption results, *i.e.*, all non-adsorbing probes reach similar uptake values when using ZIF-71 as a sorbent, and only water accessibility, determined by hydrogen-bonding ability, governs the extent of the ZIF-71 to ZIF-72 phase transition. In other words, the extent of the phase transition does not significantly affect the adsorption uptake for aniline, benzoic acid, benzaldehyde, and phenol, thereby supporting a shell-to-core transition mechanism.

Once the adsorption mechanism had been clarified, the potential of ZIF-71 was further evaluated for the removal of binary mixtures. The main goal was to identify structural changes when ZIF-71 is exposed to two different probes, with different characteristics, and at different concentrations. The aqueous medium was selected to identify the role of structural-transition promoters (*e.g.*, aniline), in hypothetical water streams containing other "adsorbing" probes (*e.g.*, fluorobenzene). The experiments were performed under two different scenarios, *i.e.*, low (50 ppm) and high (250 ppm) concentrations of aniline, and following the same procedure described in the experimental section for the individual tests. Although quantitative measurements could not be performed using UV-vis spectroscopy due to the overlap of aniline and fluorobenzene absorption bands, qualitative insights were obtained. As shown in Fig. 8, fluorobenzene (FB) is completely removed within the first 10–20 minutes (indicated by the significant decrease in the absorbance at 258 nm in both UV spectra), independently of the initial concentration of aniline (ANI) used (either 250 ppm FB–50 ppm ANI or 250 ppm FB–250 ppm ANI). These results suggest that under realistic conditions (when dealing with complex mixtures), the adsorption performance of ZIF-71 will be defined by the main component in the mixture (*e.g.*, fluorobenzene), even for mixtures with 50 : 50 with a hypothetical contaminant. In other words, small and medium concentrations of aniline (as a hypothetical contaminant) will not alter/modify the excellent adsorption performance of ZIF-71 towards fluorobenzene, highlighting the potential of ZIF-71 as a sorbent for the removal of halogenated compounds from simulated industrial streams.

Synchrotron XRD patterns of the used materials (Fig. 8e and f) confirm the above-described observations. In mixtures, the phase transition is largely suppressed at low "contaminant" concentrations (50 ppm ANI), due to the predominant role of the highly concentrated fluorobenzene, while some tiny contributions appear for "highly concentrated" aniline streams,

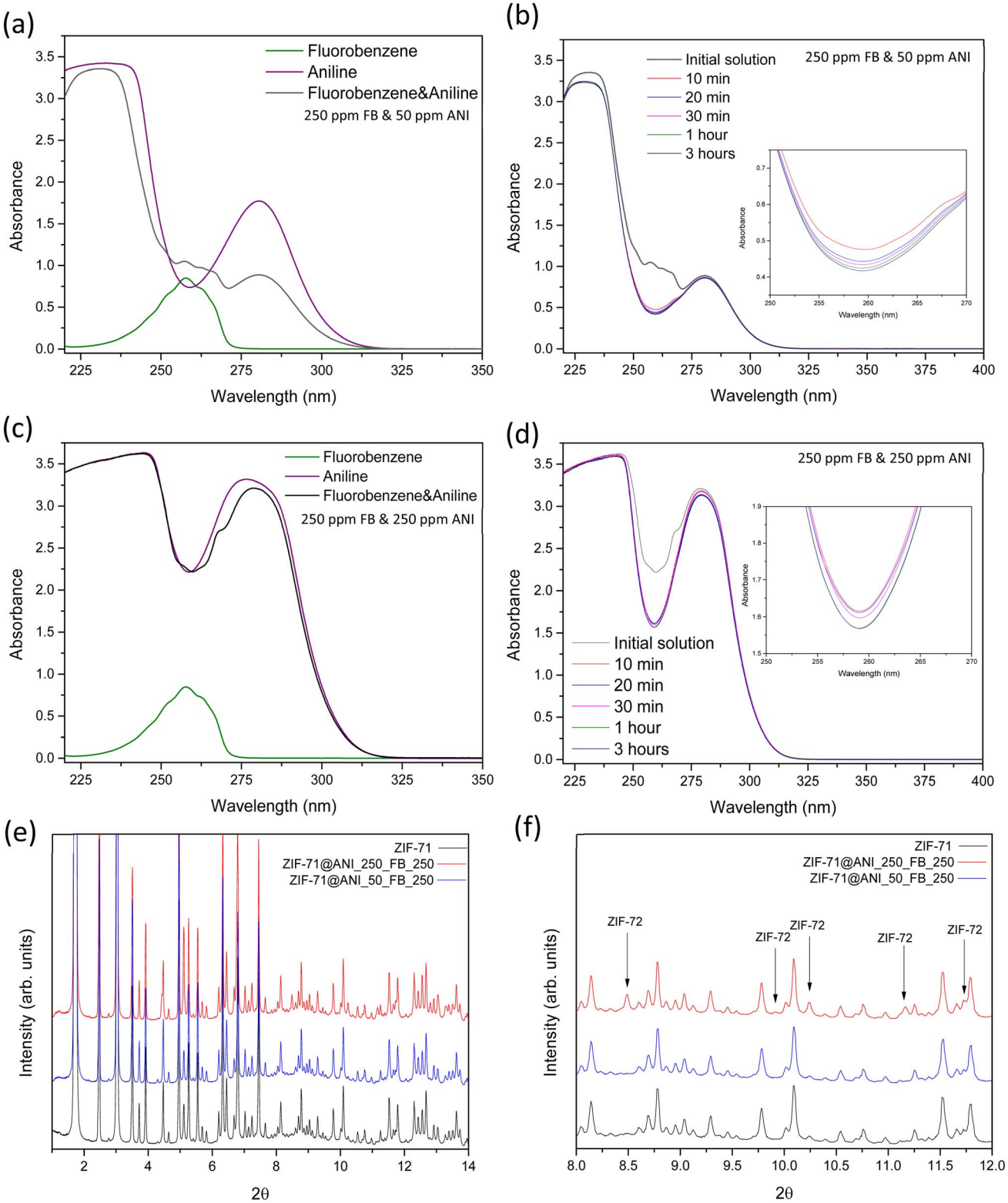

Fig. 8 (a) and (c) UV spectra of individual components (fluorobenzene (FB) and aniline (ANI)) and their corresponding mixtures at different concentrations: (a)250 ppm FB–50 ppm ANI, and (c) 250 ppm FB–250 ppm ANI; (b) and (d) UV spectra of the mixtures during the adsorption process on ZIF-71 (up to 3 h) at the two evaluated concentrations; and (e) and (f) synchrotron XRD upon the adsorption process: (e) full pattern and (f) amplification of the 8.0°–12.0° range.

although without altering/modifying the excellent adsorption performance of ZIF-71.

Conclusions

The combination of adsorption experiments, synchrotron X-ray powder diffraction (SXRPD) measurements, and Monte Carlo simulations clearly demonstrates the anomalous adsorption behavior of ZIF-71 towards volatile organic compounds. The adsorption performance of ZIF-71 can be categorized as either "adsorbing" or "non-adsorbing", depending on the physicochemical properties of the probe molecules. Synchrotron XRPD measurements confirm that non-adsorbing probes induce a distinct phase transition from the open-pore ZIF-71 to a closed-pore ZIF-72 phase. Monte Carlo simulations reveal that the key parameter governing the extent of the phase transition is the hydrogen-bonding ability; that is, probes bearing functional groups capable of strong hydrogen bonding (*e.g.*, –OH, –COOH, and $–NH_2$) facilitate the penetration of water molecules into the inner cavities of the highly hydrophobic ZIF-71, thereby accelerating the kinetically hindered transition. Beyond the fundamental interest in framework flexibility and phase transitions, these findings also highlight the potential of ZIF-71 as a selective sorbent for the removal of specific organic pollutants from aqueous media, particularly halogenated compounds. Moreover, the strong interplay between hydrogen bonding and framework dynamics unveiled in this study opens promising avenues for the rational design of MOFs with tailored sorption properties.

Conflicts of interest

There are no conflicts to declare.

Data availability

The data supporting this article are available at RUA at http://hdl.handle.net/10045/161211.

Supplementary information (SI) is available. See DOI: https://doi.org/10.1039/d5ta07361h.

Acknowledgements

J. S. A. acknowledges financial support from MCIN (Project PID2022-142960OB-C21), and Conselleria de Innovación, Universidades, Ciencia y Sociedad Digital (Project CIPROM/2021/022). Synchrotron X-ray powder diffraction measurements were performed at the Spanish ALBA synchrotron (Project AV-2024028095). J. J. G.-S. and A. M.-C. thank the Spanish Ministerio de Ciencia e Innovación for financial support (CNS2022-136163 and PID2023-152095NA-I00) and C3UPO for HPC support.

References

1 S. Seth and S. Jhulki, Porous flexible frameworks: origins of flexibility and applications, *Mater. Horiz.*, 2021, **8**, 700–727.
2 N. Behera, J. Duan, W. Jin and S. Kitagawa, The chemistry and applications of flexible porous coordination polymers, *EnergyChem*, 2021, **3**, 100067.
3 J.-P. Zhang, H.-L. Zhou, D.-D. Zhou, P.-Q. Liao and X.-M. Chen, Controlling flexibility of metal-organic frameworks, *Natl. Sci. Rev.*, 2018, **5**, 907–919.
4 N. J. Corrente, S. Parashar, R. Gough, E. L. Hinks, P. I. Ravikovith and A. V. Neimark, Modeling structural flexibility in 3D carbon models: a hybrid MC/MD approach to adsorption-induced deformation, *Carbon*, 2025, **238**, 120160.
5 J. J. Gutierrez-Sevillano, S. Calero, S. Hamad, R. Grau-Crespo, F. Rey, S. Valencia, M. Palomino, S. R. G. Balestra and A. R. Ruiz-Salvador, Critical role of dynamic flexibility in Ge-containing zeolites: impact of diffusion, *Chem.–Eur. J.*, 2016, **22**, 10036–10043.
6 P. I. Ravikovitch and A. V. Neimark, Density functional theory model of adsorption deformation, *Langmuir*, 2006, **22**, 10864–10868.
7 C. Balzer, A. M. Waag, S. Gehret, G. Reichenauer, F. Putz, N. Hüsing, O. Paris, N. Bernstein, G. Y. Gor and A. V. Neimark, Adsorption-induced deformation of hierarchically structured mesoporous silica-effect of the pore-level anisotropy, *Langmuir*, 2017, **33**, 5592–5602.
8 D. Fairen-Jimenez, S. A. Moggach, M. T. Wharmby, P. A. Wright, S. Parsons and T. Düren, Opening the gate: framework flexibility in ZIF-8 explored by experiments and simulations, *J. Am. Chem. Soc.*, 2011, **133**, 8900–8902.
9 A. Noguera-Díaz, J. Villaroel-Rocha, V. P. Ting, N. Bimbo, K. Sapag and T. J. Mays, Flexible ZIFs: probing guest-induced flexibility with CO_2, N_2 and Ar adsorption, *J. Chem. Technol. Biotechnol.*, 2019, **94**, 3787–3792.
10 M. E. Casco, Y. Q. Cheng, L. L. Daemen, D. Fairen-Jimenez, E. V. Ramos-Fernández, A. J. Ramirez-Cuesta and J. Silvestre-Albero, Gate-opening effect in ZIF-8: the first experimental proof using inelastic neutron scattering, *Chem. Commun.*, 2016, **52**, 3639–3642.
11 C. Cuadrado-Collados, J. Fernandez-Catala, F. Fauth, Y. Q. Cheng, L. L. Daemen, A. J. Ramirez-Cuesta and J. Silvestre-Albero, Understanding the breathing phenomena in nano-ZIF-7 upon gas adsorption, *J. Mater. Chem. A*, 2017, **5**, 20938–20946.
12 Y. Du, K. Mao, B. Wooler, A. K. Sharma, D. Colmyer, M. Nines and S. C. Weston, Insights into the flexibility of ZIF-7 and its structural impact in alcohol adsorption, *J. Phys. Chem. C*, 2017, **121**, 28090–28095.
13 J. Gandara-Loe, A. Missyul, F. Fauth, L. L. Daemen, Y. Q. Cheng, A. J. Ramirez-Cuesta, P. I. Ravikovitch and J. Silvestre-Albero, New insights into the breathing phenomenon in ZIF-4, *J. Mater. Chem. A*, 2019, **7**, 14552–14558.
14 K. Dedecker, M. Drobek and A. Julbe, Selective adsorption and separation of C_6 hydrocarbons: the role of structural flexibility and functionalization in zeolitic imidazolate frameworks, *RSC Appl. Interfaces*, 2024, **2**, 364–372.

15 N. Aljammal, C. Jabbour, S. Chaemchuen, T. Juzsakova and F. Verpoort, Flexibility in metal-organic frameworks: a basic understanding, *Catalysts*, 2019, **9**, 512.
16 G. Chaplais, G. Fraux, J.-L. Paillaud, C. Marichal, H. Nouali, A. H. Fuchs, F.-X. Coudert and J. Patarin, Impacts of the imidazolate linker substitution (CH_3, Cl, or Br) on the structural and adsorptive properties of ZIF-8, *J. Phys. Chem. C*, 2018, **122**, 26945–26955.
17 R. Bose, V. Bon, N. Bönisch, P. Selvam, N. S. Kaisare and S. Kaskel, Crystal size dependent flexibility in ZIF-7: from macro- to nanoscale, *Chem. Mater.*, 2023, **35**, 7825–7838.
18 A. B. Ekanayake, A. A. Tiba, L. R. MacGillivray and A. V. Tivanski, Crystal size-dependent framework flexibility of a prototypical metal organic framework is related to metal content: zeolitic imidazolate framework-7, *Mater. Adv.*, 2024, **5**, 9055–9060.
19 A. Henschel, I. Senkovska and S. Kaskel, Liquid-phase adsorption on metal-organic frameworks, *Adsorption*, 2011, **17**, 219–226.
20 E. Amayuelas, J. Farrando-Perez, A. Missyl, Y. Grosu, J. Silvestre-Albero and C. Carrillo-Carrión, Fluorinated nanosized zeolitic-imidazolate frameworks as potential devices for mechanical energy storage, *ACS Appl. Mater. Interfaces*, 2024, **16**, 46374–46383.
21 Y. Sun, Y. Li and J.-C. Tan, Framework flexibility of ZIF-8 under liquid intrusion: discovering time-dependent mechanical response and structural relaxation, *Phys. Chem. Chem. Phys.*, 2018, **20**, 10108–10113.
22 J. Farrando-Perez, A. Missyul, A. Martín-Calvo, C. Abreu-Jauregui, V. Ramirez-Cerezo, L. Daemen, Y. Q. Cheng, A. J. Ramirez-Cuesta, S. Calero, C. Carrillo-Carrión and J. Silvestre-Albero, Molecular recognition-induced structural flexibility in ZIF-71, *J. Mater. Chem. A*, 2024, **12**, 28975–28984.
23 D. Dubbeldam, S. Calero, D. E. Ellis and R. Q. Snurr, RASPA: molecular simulation software for adsorption and diffusion in flexible nanoporous materials, *Mol. Simul.*, 2015, **42**, 81–101.
24 B. Widom, Some topics in the theory of fluids, *J. Chem. Phys.*, 1963, **39**, 2808–2812.
25 S. Kim, J. Chen, T. Cheng, A. Gindulyte, J. He, S. He, Q. Li, B. A. Shoemaker, P. A. Thiessen, B. Yu, L. Zaslavsky, J. Zhang and E. E. Bolton, PubChem 2023 update, *Nucleic Acids Res.*, 2023, **51**, D1373–D1380.
26 N. Rai and J. I. Siepmann, Transferable potentials for phase equilibria. 10. Explicit-hydrogen description of substituted benzenes and polycyclic aromatic compounds, *J. Phys. Chem. B*, 2013, **117**, 273–288.
27 H. J. C. Berendsen, J. R. Grigera and T. P. Straatsma, The missing term in effective pair potentials, *J. Phys. Chem.*, 1987, **91**, 6269–6271.
28 D. K. J. A. Wanigarathna, J. Gao and B. Liu, Metal organic frameworks for adsorption-based separation of fluorocompounds: a review, *Mater. Adv.*, 2020, **1**, 310–320.
29 M. Mezei and D. L. Beveridge, Theoretical studies of hydrogen bonding in liquid water and dilute aqueous solutions, *J. Chem. Phys.*, 1981, **74**, 622–632.
30 A. Luzar and D. Chandler, Effect of environment on hydrogen bond dynamics in liquid water, *Phys. Rev. Lett.*, 1996, **76**, 928.
31 A. Luzar and D. Chandler, Structure and hydrogen bond dynamics of water-dimethyl sulfoxide mixtures by computer simulations, *J. Chem. Phys.*, 1993, **98**, 8160–8173.
32 A. Luzar and D. Chandler, Hydrogen-bond kinetics in liquid water, *Nature*, 1996, **379**, 55–57.
33 D. Swiatla-Wojcik, Evaluation of the criteria of hydrogen bonding in highly associated liquids, *Chem. Phys.*, 2007, **342**, 260–266.
34 M. Tu, D. E. Kravchenko, B. Xia, V. Rubio-Gimenez, N. Wauteraerts, R. Verbeke, I. F. J. Vankelecom, T. Stassin, W. Egger, M. Dickmann, H. Amenitsch and R. Ameloot, Template-mediated control over polymorphism in the vapor-assisted formation of zeolitic imidazolate framework powders and films, *Angew. Chem., Int. Ed.*, 2021, 7553–7558.

